crystals

MDPI

Article

Combining a Drug and a Nutraceutical: A New Cocrystal of Praziquantel and Curcumin

Camila Caro Garrido [1,*], Marie Vandooren [1], Koen Robeyns [1], Damien P. Debecker [1], Patricia Luis [2] and Tom Leyssens [1,*]

[1] Institute of Condensed Matter and Nanosciences, UCLouvain, 1 Place Louis Paster, B-1348 Louvain-la-Neuve, Belgium; marie.vandooren@student.uclouvain.be (M.V.); koen.robeyns@uclouvain.be (K.R.); damien.debecker@uclouvain.be (D.P.D.)

[2] Institute of Mechanics, Materials and Civil Engineering, UCLouvain, 2 Place Sainte Barbe, B-1348 Louvain-la-Neuve, Belgium; patricia.luis@uclouvain.be

* Correspondence: camila.carogarrido@uclouvain.be (C.C.G.); tom.leyssens@uclouvain.be (T.L.); Tel.: +32-497-881-129 (C.C.G.); +32-104-728-11 (T.L.)

Abstract: This study explores the co-crystallization between the drug praziquantel (PZQ) and the nutraceutical curcumin (CU). The investigation revealed two novel solid forms: a cocrystal solvate with ethyl acetate and a non-solvated cocrystal. This novel drug–nutraceutical cocrystal is a praziquantel–curcumin (2:1) cocrystal. The cocrystal solvate has ethyl acetate molecules occupying the voids with minimal interactions within the crystal lattice. The application of heat treatment induces solvent removal and prompts the transition to the non-solvated cocrystal, as highlighted by variable-temperature X-ray powder diffraction (VT-XRPD). Thermal analyses demonstrate the stability of the cocrystal solvate up to approximately 100 °C, beyond which it transforms into the non-solvated phase, which eventually melts at 130 °C.

Keywords: praziquantel; curcumin; nutraceutical; coformer; cocrystal solvate; cocrystal

check for updates

Citation: Garrido, C.C.; Vandooren, M.; Robeyns, K.; Debecker, D.P.; Luis, P.; Leyssens, T. Combining a Drug and a Nutraceutical: A New Cocrystal of Praziquantel and Curcumin. *Crystals* **2024**, *14*, 181. https://doi.org/10.3390/cryst14020181

Academic Editor: Aidar T. Gubaidullin

Received: 7 January 2024
Revised: 5 February 2024
Accepted: 8 February 2024
Published: 11 February 2024

Copyright: © 2024 by the authors. Licensee MDPI, Basel, Switzerland. This article is an open access article distributed under the terms and conditions of the Creative Commons Attribution (CC BY) license (https://creativecommons.org/licenses/by/4.0/).

1. Introduction

Praziquantel (PZQ), marketed as ^{Pr}BILTRICIDE® by Bayer, is an acylated quinoline–pyrazine derivative (Figure 1). It is the most effective and widely administered first-line and broad-spectrum anthelmintic drug in both humans and animals. This medicine is used against all *Schistosoma* spp. for control and (preventive) treatment [1]. Schistosomiasis, or bilharzia, is an acute and chronic water-based disease caused by parasitic trematode flatworms [2]. This tropical disease has considerable morbidity worldwide, particularly in sub-Saharan Africa, and school-aged children (aged 5 to 14 years) are recognized as especially vulnerable to this infection [3]. Human beings are contaminated by infested water during routine actions such as domestic, occupational, agricultural, and recreational activities. This disease essentially affects populations that do not have access to potable water. In 2021, more than 250 million people needed preventive treatment [4]. This explains why PZQ is enlisted in the World Health Organization's (WHO) Model List of Essential Medicines [5].

Praziquantel is a chiral compound and is commercially marketed as a racemate (*RS*-PZQ). However, the schistosomicidal activity mainly comes from the (*R*)-enantiomer (*R*-PZQ) [6]. This means that only half of the administered drug contributes to the therapeutic activity. Moreover, (*S*)-enantiomer (*S*-PZQ) is responsible for the bitter taste of praziquantel [7]. Furthermore, *RS*-PZQ exhibits poor solubility in aqueous media (0.40 mg/mL in water at 25 °C) and consequently shows poor bioavailability, imposing the requirement for high clinical doses (large tablets of 600 mg) [8]. The tablet's dimension and the unpleasant taste of praziquantel, even as a syrup or crushed and mixed with juice, are challenging for children, who form the largest patient group [9].

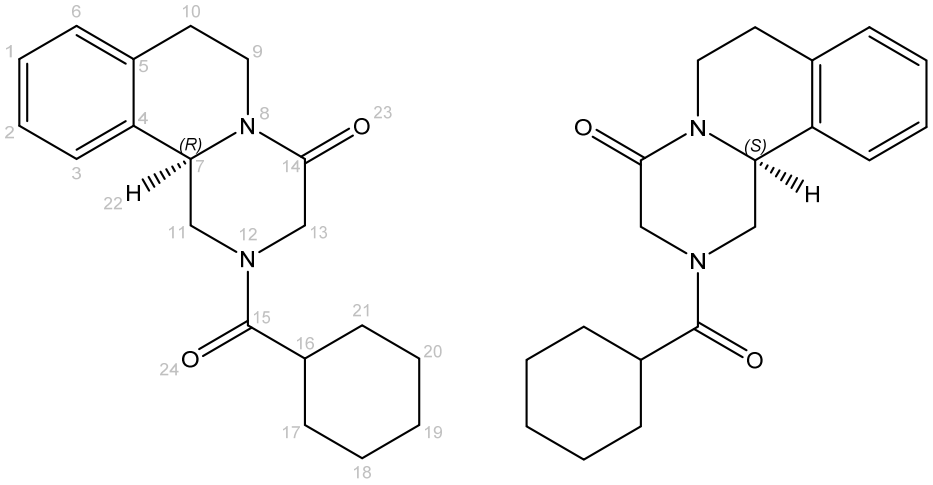
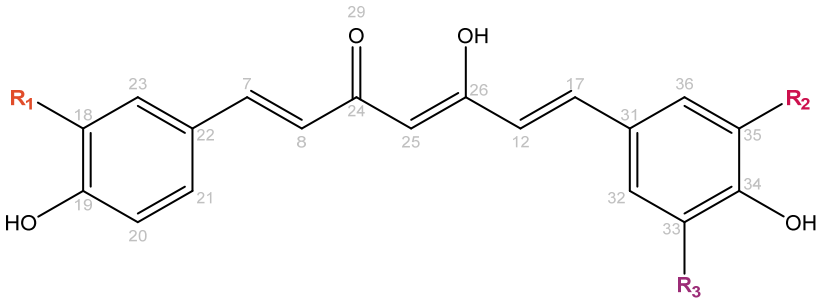


Figure 1. Molecular structures of *R*- and *S*-PZQ enantiomers. Atom numbers are colored in gray.

A common approach in crystal engineering to enhance API properties, such as low water solubility, low dissolution rate, or low chemical stability, is to screen for alternative solid forms, such as amorphous phases [10], polymorphs [11], salts [12], and/or cocrystals [13], all showing a variation in lattice energy and hence pharmaceutical properties. The issues related to praziquantel make searching for new solid forms relevant. Since PZQ has no ionizable group, it is unsuitable for salt formation. It does, however, feature two carbonyl groups capable of functioning as hydrogen bond acceptors, making them excellent candidates for cocrystal formation [14]. To date, 3 polymorphs [14–16], 3 solvates [17,18], and 31 cocrystals [14,19–23] of *RS*-PZQ have been reported in the CCDC (Cambridge Crystallographic Data Center) database. Based on the analysis of these structures, *RS*-PZQ shows a multitude of cocrystals involving carboxylic acid co-formers (e.g., oxalic acid, malonic acid, malic acid, etc.) or compounds containing polyphenol hydroxyl groups (e.g., ferulic acid, kaempferol, quercetin, etc.) [24]. We, therefore, selected curcumin (CU), a well-studied natural polyphenol and a nutraceutical with a ginger-like taste, as a potential cocrystal former for *RS*-PZQ.

Curcumin (Figure 2) is an intense yellow–orange polyphenolic pigment extracted from the turmeric rhizome, belonging to the ginger family. This bioactive molecule is also known as food additive E100 and has numerous applications as a flavoring agent, coloring agent, food preservative, and dietary supplement [25]. It is also considered a nutraceutical, a substance of natural origin that extends its usefulness beyond basic nutritional functions [26]. Curcumin is the main pharmacologically active constituent of turmeric among curcuminoids (demethoxycurcumin, bisdemethoxycurcumin, etc.) [27]. It is used in traditional medicine and is claimed to have many pharmacological effects (such as antioxidant, anti-inflammatory, antimicrobial, etc., effects) [28,29]. Curcumin shows keto-enol tautomerism and can interact with various targets (protein kinases, transcription factors, etc.) [30]. Despite being a GRAS (generally recognized as safe) compound, it has very poor aqueous solubility (0.6 μg/mL in pure water at RT) and low bioavailability, limiting its therapeutic effectiveness [31]. Previous studies have shown curcumin to co-crystallize with co-formers such as resorcinol, pyrogallol, cinnamic acid, resveratrol, salicylic acid, and hydroxyquinol [32–35].

Here, we aimed to modify *RS*-PZQ properties by forming a new drug–nutraceutical cocrystal [36,37] with curcumin. Such a cocrystal could potentially reduce the bitter taste of praziquantel tablets and could potentially impact the adverse effects of the drug (headache, abdominal pain, muscle pain, fatigue, and weakness) [1,9].



Curcumin (CU): $R_1 = -OCH_3$, $R_2 = -OCH_3$, $R_3 = -H$
Demethoxycurcumin (DMC): $R_1 = -H$, $R_2 = -H$, $R_3 = -OCH_3$
Bis(demethoxy)curcumin (BDMC): $R_1 = -H$, $R_2 = -H$, $R_3 = -H$

Figure 2. Molecular structures of turmeric's main curcuminoids, represented as enol forms. Atom numbers are colored in gray.

2. Materials and Methods

2.1. Materials

Synthetic curcumin (CAS: 458-37-7, >97.0%) and racemic praziquantel (CAS: 55268-74-1, >98.0%) were acquired from TCI EUROPE N.V. (Zwijndrecht, Belgium). Solvents were acquired from VWR International BV (Brecht, Belgium). All materials were used as received without any further purification.

2.2. Cocrystal Screening through Liquid-Assisted Grinding (LAG) Experiments

Screening of cocrystals between curcumin and racemic praziquantel was performed using liquid-assisted grinding (LAG) in the MM 400 Mixer Mill grinder manufactured by RETSCH (Haan, Germany). The latter is equipped with two grinding jars that can each contain 5 Eppendorf tubes of 2 mL. Each tube was filled with an equimolar quantity (0.4 mmol) of curcumin and racemic praziquantel and 100 µL of toluene as well as 4 small stainless-steel beads (Ø 3 mm). The grinding program was set for 90 min at a beating frequency of 30 Hz. The resulting ground powders were studied via X-ray powder diffraction (XRPD).

2.3. Congruency Experiments

Congruency experiments were carried out via slurry crystallization. At first, slurry experiments were prepared by suspending an equimolar amount (0.3 mmol) of racemic praziquantel and curcumin in a suitable amount of solvent (from 1 to 4 mL). The solvents tested include 2-propanol (IPA), acetonitrile (ACN), ethanol (EtOH), ethyl acetate (EtOAc), and methanol (MeOH). The suspensions were shaken at 150 rpm for 3 to 4 days at room temperature (RT) in 5 mL sealed vials using the "Orbital Shaker SO3" from Stuart Scientific. The powders were then filtered, washed with fresh solvent, dried, and analyzed via X-ray powder diffraction.

Then, slurry experiments were carried out using a 2:1 ratio of racemic praziquantel (0.6 mmol) and curcumin (0.3 mmol) in a suitable amount of ethyl acetate (from 1 to 4 mL). The suspensions were also shaken at 150 rpm for 3 to 4 days at RT in 5 mL sealed vials using the "Orbital Shaker SO3" from Stuart Scientific. The powders were then filtered, washed with fresh ethyl acetate, dried, and analyzed by XRPD. This provided the bulk material. Trials were performed with various solvents to obtain the non-solvated bulk material, but these attempts were unsuccessful.

2.4. Single Crystal Growth

Single crystals were grown through slow evaporation and cooling of the supernatants retrieved from the slurry experiments (prepared as previously described using a 2:1 ratio of racemic praziquantel and curcumin in EtOAc). Concerning the slow evaporation

experiments, the supernatants were left to evaporate slowly from 3 to 10 days at +/− RT. For the single crystals formed through cooling, the supernatants retrieved from the slurry experiments were placed in a refrigerator at −4 °C. Suitable crystals of the 2:1: praziquantel–curcumin–ethyl acetate cocrystal solvate were successfully obtained both from cooling and the slow evaporation experiments. Trials were performed with various solvents to obtain the non-solvated single cocrystal, but these attempts were unsuccessful.

2.5. X-ray Powder Diffraction (XRPD)

X-ray diffraction measurements were carried out using a Siemens D5000 diffractometer from Bruker Belgium, furnished with a Cu cathode (with a wavelength of λ = 1.5418 Å) running at 40 kV and 40 mA and employing a Bragg–Brentano geometry. X-ray patterns were recorded in 2θ angle values, in the scanning range from 5 to 35°, with a step size of 0.02° and an integration time of 2 s (rate of 0.6°/min). Patterns of known starting compounds were simulated from the single crystal structures using Mercury 4.2.0 software [38]. The obtained X-ray diffraction patterns were analyzed using WinPLOTR software [39].

2.6. Single Crystal X-ray Diffraction Analysis (SCXRD)

Single crystal X-ray diffraction data were collected on a MAR345 image plate detector using Mo Kα radiation from an Incoatec microfocus source (Montel mirrors). CrysAlis^{PRO} software was used to integrate the images, and the implemented absorption correction was applied [40]. The structure solution was produced using dual space direct methods (SHELXT) [41], and the structure was then refined against F^2 using SHELX-2018/3 [42]. All non-hydrogen atoms were anisotropically refined, and hydrogens were placed at calculated positions in riding mode with Ueq set at 1.2 times the Ueq of the parent atoms (1.5 for OH hydrogens). The keto-enol equilibrium at the center of the curcumin molecule results in an intra-molecular H-bond with the hydrogen located on either of the two central oxygens. To properly account for this tautomerism, hydrogen at 50% occupancy was added to both oxygens, geometrically placed to form an intra-molecular H-bond. PLATON allowed for the symmetry analysis and validation of the structure [43]. The figures were made using the molecular visualization software Mercury 4.2.0 [38].

To obtain (non-solvated) 2:1 praziquantel–curcumin cocrystals, a single crystal of 2:1:1 praziquantel–curcumin–ethyl acetate cocrystal solvate was mounted in a glass capillary and placed in an N_2-flow of an Oxford Cryostream set at RT. The system was heated from RT to 370 K at 3 °C/min and then heated further from 370 K to 390 K at 2 °C/min. Unit cell determination was performed at 380 K and 390 K to follow the crystal-to-crystal transformation. Finally, the crystal inside the capillary was cooled down to 298 K at 4 °C/min. SCXRD data were collected on the crystal inside the capillary and treated as previously described. Due to the heat treatment and the subsequent solvent removal, leading to a phase transformation, the quality of the single crystal deteriorated significantly, resulting in a lower resolution limit.

2.7. Variable Temperature X-ray Diffraction (VT-XRD)

XRPD patterns were measured in glass capillaries with a diameter of 0.7 mm (Hilgenberg GmbH, Malsfeld, Germany). The analysis involved a MAR345 image plate detector (sample–detector distance, 200 mm) and a microfocus Incoatec Source (IμS) Mo (Montel mirror) source operating at 50 kV and 600 μA. The sample was exposed for 5 min while the capillary containing the sample was rotated by 180°. Diffraction data were integrated using Fit2D software, (with data obtained from a 0.1 mm diameter capillary filled with LaB6 as a calibrant). For variable-temperature X-ray powder diffraction (VT-XRPD), the sample-filled capillary was heated using a Cryostream 800PLUS, Oxford Cryosystems, Sarsden, UK.

A capillary filled with the cocrystal solvate was heated at 3 K/min to 380 K. The sample was allowed to equilibrate for a few minutes, and an XRD pattern was recorded. Subsequent PXRD patterns were recorded after 2 K/min heating ramps at 385 and 395 K.

2.8. Thermogravimetric Analysis (TGA)

TGA measurements were carried out using a Mettler Toledo TGA-STDA 851e. Approximately 5 to 10 mg of sample were placed in an aluminum oxide crucible, and the temperature was ramped from 25 °C to 600 °C at a heating rate of 5 °C/min. The purge gas was nitrogen, with a continuous flow rate of 50 mL/min. The data were treated with STARe 12.12 software.

2.9. Differential Scanning Calorimetry (DSC) Analysis

Differential scanning calorimetry measurements were conducted using a TA DSC2500. A sample mass of approximately 5 to 10 mg was placed in an aluminum Tzero pan with a perforated hermetic lid, and the temperature was scanned at a rate of 5 °C/min: first heating from 25 °C to 150 °C, then cooling from 150 °C to 25 °C, to eventually finishing the cycle with a second heating period from 25 to 220 °C. The purge gas was nitrogen, with a continuous flow rate of 50 mL/min. The data were treated with TA Instruments Trios V5.1.1.46572 software.

2.10. Proton Nuclear Magnetic Resonance (^{1}H NMR)

Proton nuclear magnetic resonance spectra were recorded on a Bruker 300 MHz spectrometer. The powders obtained from the slurry experiments were solubilized in DMSO-d^6. ^{1}H NMR chemical shifts are reported in parts per million (ppm) relative to the chemical shift of the peak of the deuterated solvent used ($(CD_3)_2SO$; 2.50 ppm). Spectral multiplicities are noted as follows: singlet = s, doublet = d, triplet = t, quartet = q, and multiplet = m.

3. Results and Discussion

3.1. Cocrystal Identification

Praziquantel has two amide groups that have the capacity to establish robust hydrogen bonding interactions. We opted for curcumin (CU), a well-studied natural polyphenol, as our choice for generating cocrystals with racemic praziquantel. The selection of curcumin is motivated by its potential to form non-covalent intermolecular interactions, particularly hydrogen bonds, thus potentially facilitating the creation of supramolecular synthons.

Screening experiments were conducted to search for new co-crystalline phases of racemic praziquantel using the liquid-assisted grinding method. A potential novel solid phase was identified through X-ray powder diffraction analysis (Figure 3). Comparison of the XRPD patterns of racemic praziquantel, curcumin, and the solid obtained from the toluene LAG experiment indicates that CU and *RS*-PZQ generated a new solid form significantly different from the known forms of the starting materials. However, the diffractogram of the solids resulting from the LAG experiment shows peaks of unreacted curcumin, suggesting that a new potential solid form exists in a ratio other than a 1:1 ratio.

1:1 slurry experiments were performed in isopropanol, acetonitrile, ethanol, methanol, and ethyl acetate (EtOAc). For all but the latter, curcumin was obtained in suspension (Figure S1). The slurry from ethyl acetate shows a pattern different from the parent compounds (Figure S1). Single crystals were therefore sought using this solvent in 1:1, 2:1, and 1:2 ratios. The 2:1 ratio led to the formation of a praziquantel–curcumin-ethyl acetate cocrystal solvate (PZQ-CU-EtOAc 2:1:1). As will be shown later on, this phase can be desolvated, leading to the praziquantel–curcumin cocrystal (PZQ-CU 2:1), also identified during the toluene LAG experiment (Figure 3).

The main crystallographic parameters are compared in Table 1, with a detailed discussion of each solid form provided below. Complete crystallographic data can be found in the Supporting Information (SI), specifically in Table S1. Additionally, PZQ-CU-EtOAc 2:1:1 cocrystal solvate SCXRD was also measured at RT (Table S2).

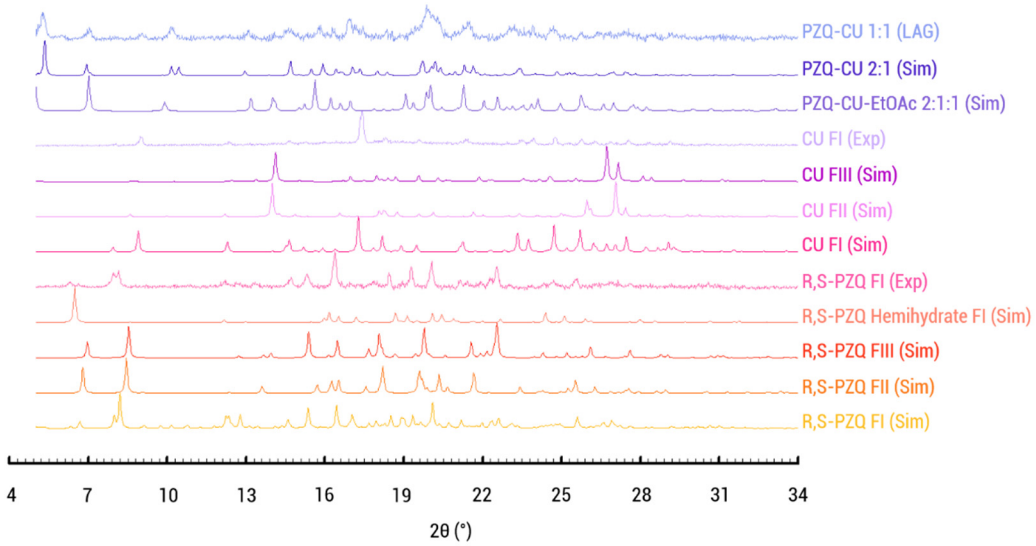


Figure 3. Normalized diffraction patterns. Simulated diffraction pattern of the known polymorphs (FI-III) and hemihydrate of the parent compounds racemic praziquantel and curcumin, praziquantel–curcumin–ethyl acetate cocrystal solvate (PZQ-CU-EtOAc 2:1:1), and praziquantel–curcumin cocrystal (PZQ-CU 2:1) and the experimental patterns of the parent's compounds used as well as the powder obtained via toluene LAG. Curcumin is shown to match with FI, whereas the praziquantel parent compound matches with the simulated pattern of FI.

Table 1. Main crystallographic parameters of the praziquantel–curcumin-ethyl acetate (2:1:1) cocrystal solvate and the praziquantel–curcumin (2:1) cocrystal.

	PZQ-CU-EtOAc (2:1:1)	**PZQ-CU (2:1)**
Formula	$C_{21}\ H_{20}\ O_6$, ·2($C_{19}\ H_{24}\ N_2\ O_2$), ·$C_4\ H_8\ O_2$	$C_{21}\ H_{20}\ O_6$, ·2($C_{19}\ H_{24}\ N_2\ O_2$)
MW (g/mol)	1081.27	993.20
T (K)	150 (2)	297 (2)
Crystal system	Monoclinic	Monoclinic
Space group	*C*2/*c*	$P2_1/n$
a, b, and c (Å)	37.570 (2), 5.9187 (3), 26.6434 (17)	27.330 (4), 5.8708 (7), 35.486 (7)
β (°)	110.574 (7)	111.06 (2)
Cell volume (Å^3)	5546.6 (6)	5313.5 (17)
Z	4	4
CCDC	2309015	2309017

3.2. Structural and Thermal Characterization

As shown in Table 1, PZQ-CU-EtOAc (2:1:1) crystallizes in the C-centered monoclinic space group *C*2/*c* and comprises four formula units within its unit cell. It presents itself as a stoichiometric solvate. Ethyl acetate molecules exhibit limited interactions within the crystal lattice; they primarily occupy the voids in the structure and exert minimal influence on its packing arrangement, as shown in Figure 4. Furthermore, these solvent molecules are found disordered on an inversion center and lack stabilization interactions. The PZQ molecules adopted an anti-conformation of the C=O groups of the piperazinone–cyclohexylcarbonyl segment. Curcumin molecules are located on a two-fold axis and additionally show whole-molecule disorder (91/9 ratio for the structure determined at 150 K; 85/15 ratio for the structure determined at RT) within the crystal lattice and present strong intramolecular O-H—O=C hydrogen bonds involving the enol group, which is preserved for the disordered molecules. This hydrogen bond has an $S_1^1(6)$ intramolecular hydrogen bond pattern, according to Etter's graph-set notation [44] (following descriptor *a* in Figure 4). Praziquantel and curcumin molecules are linked by two hydrogen bonds, giving a molecular assembly of the composition PZQ---CU---PZQ. These latter interactions

result in two $D_1^1(2)$ finite patterns coupled into one $D_2^2(21)$ finite pattern, involving the -OH group of curcumin and the C=O function of the cyclohexylcarbonyl group of praziquantel, following the *b* descriptor through the <*b* >*b* path.

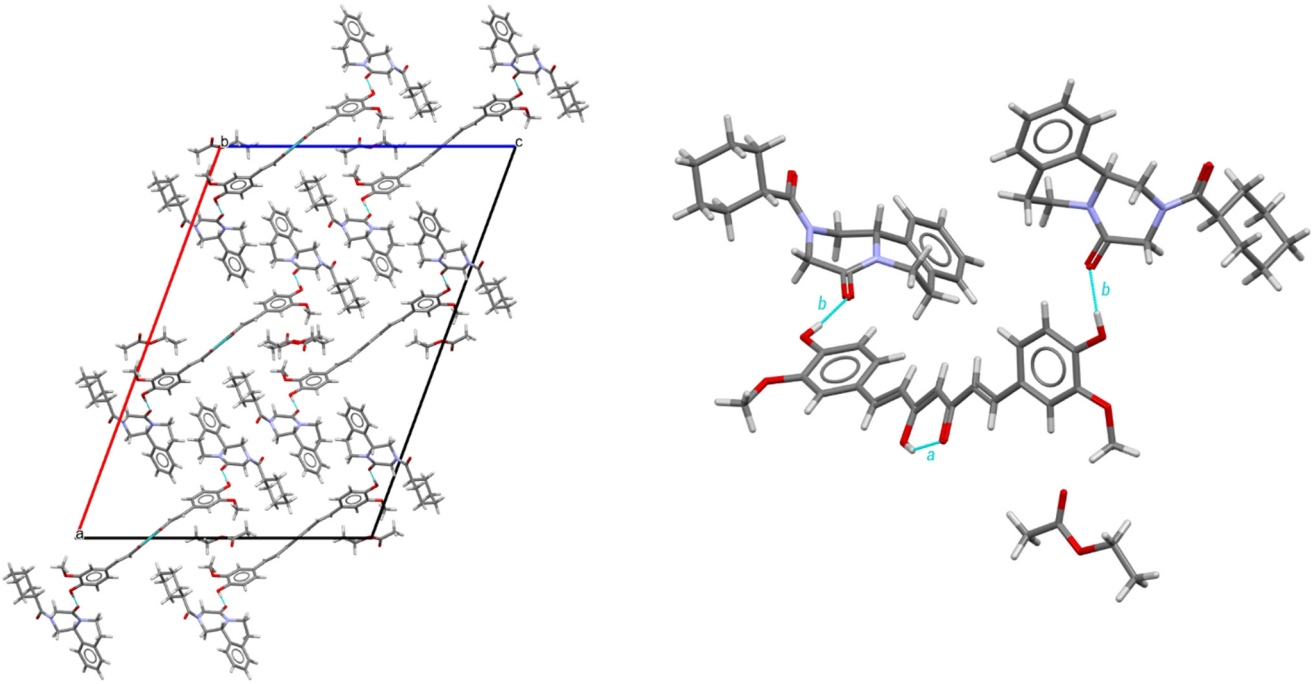


Figure 4. Structure of the PZQ–CU–EtOAc (2:1:1) cocrystal solvate. On the left: crystal packing, viewed along the b-axis; on the right: hydrogen bond arrangement, viewed along the origin. For the disordered molecules only, the major part is represented.

The bulk material of the cocrystal solvate can be obtained from a 2:1 slurry experiment in ethyl acetate at room temperature (see Supporting Information, Figure S1). The ^{1}H NMR analysis (see Supporting Information, Figure S3) confirms the 2:1:1 stoichiometry of this novel cocrystal solvate composed of praziquantel, curcumin, and ethyl acetate, given that the integration of peaks furnishes insights into the relative abundance of distinct nuclei within the sample. For example, in the cocrystal solvate sample, the ethyl acetate singlet at 1.99 ppm integrates for three protons representing the -OCH_3 group, curcumin doublets at 7.57 and 7.53 ppm each integrate for two protons, corresponding to both symmetrical ethylene -CH groups (denoted as 7, 8, 12, 17 in Figure 2), and the praziquantel multiplet at 1.46–1.22 ppm integrates for 10 protons (and not 5 protons such as in the case of a single equivalent of PZQ), corresponding to the -CH protons of the cyclohexane group in anti-conformation denoted as 17 to 21 in Figure 1.

Due to the loosely bound ethyl acetate molecules, the cocrystal solvate can be desolvated in a single-crystal-to-single-crystal transition. The **praziquantel–curcumin (2:1) cocrystal** structure was thus obtained by slowly heating a single crystal from RT to 370 K at 3 °C/min, then at a slower heating rate of 2 °C/min from 370 K to 390 K, and finally cooling down to 298 K at 4 °C/min. PZQ–CU (2:1) was found to crystallize in the primitive monoclinic space group $P2_1/n$ and contains four molecules per unit cell. The comparison of the unit cell parameters of the cocrystal solvate and the cocrystal in Table 1 shows these two solid forms to be slightly different, leading to some differences in the XRPD patterns (Figure 3). The crystal lattices indeed exhibit a high degree of similarity (Figure 5), with solvent removal leading to a slight crystal lattice volume reduction.

In the praziquantel–curcumin (2:1) cocrystal, the dominant supramolecular interactions are therefore similar to the ones in the cocrystal solvate, as shown in Figure 6. Curcumin molecules form strong intramolecular O-H---O hydrogen bonds following an $S_1^1(6)$ intramolecular hydrogen bond pattern. Two *R*- (or two *S*-) praziquantel molecules

are connected to 1 curcumin by two hydrogen bonds, combined in two $D_1^1(2)$ finite patterns merged into one $D_2^2(21)$ finite pattern. The molecular assembly PZQ–CU–PZQ involves the hydroxy group of curcumin and the carbonyl function of the cyclohexylcarbonyl group of praziquantel, following the *b* and *c* descriptors along the <*b* >*c* path.

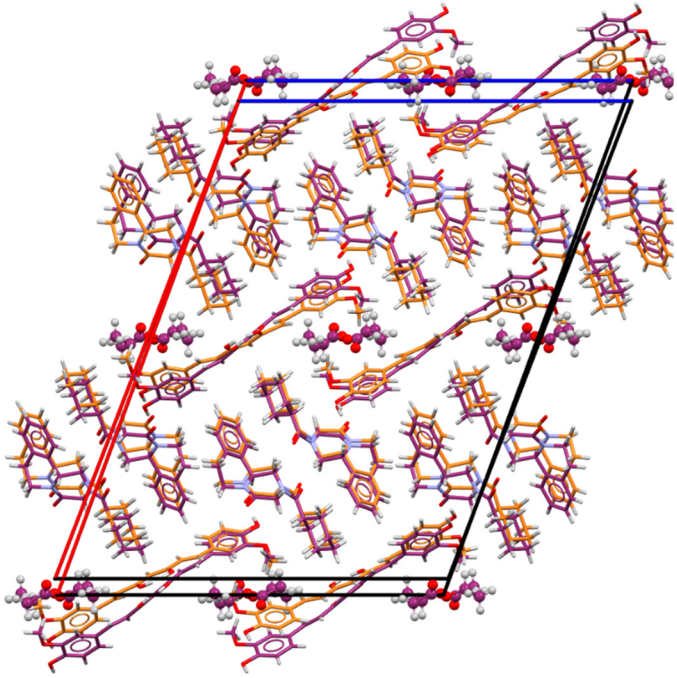


Figure 5. Packing superposition of the 2:1:1 PZQ-CU-EtOAc cocrystal solvate (carbon atoms in dark purple) and the 2:1 PZQ-CU cocrystal (carbon atoms in orange), viewed along the b-axis (without disorder).

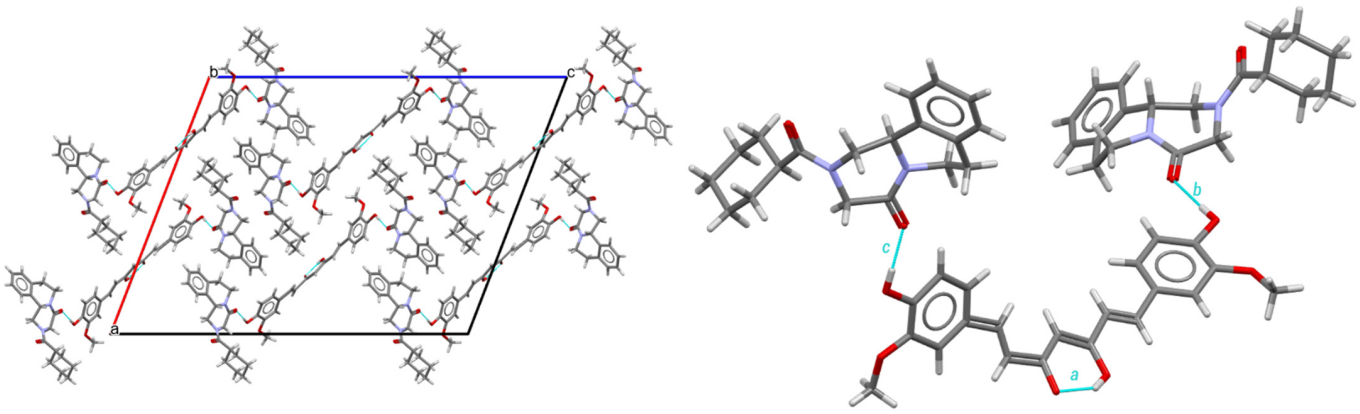


Figure 6. Structure of the PZQ–CU (2:1) cocrystal. Left: crystal packing, viewed along the b-axis; right: hydrogen bond arrangement.

As shown in Figure 3, the simulated XRPD pattern of the praziquantel–curcumin (2:1) cocrystal closely matches the experimental pattern obtained via liquid-assisted grinding with toluene, with the experimental pattern showing some parent compound remaining.

Thermogravimetric analysis (Figure 7) showed the praziquantel–curcumin–ethyl acetate (2:1:1) cocrystal solvate to be stable up to approximately 100 °C, at which point weight loss of 7% was observed, which closely aligns with the theoretically expected weight loss of a single ethyl acetate molecule from the cocrystal solvate (theoretical value of 8.15%). The DSC analysis conducted using a heating rate of 5 °C/min (Figure 8) also showed this desolvation as an endothermic peak with T_{onset} = 101.90 °C (T_{peak} = 113.32 °C)

and a heat of desolvation of ΔH = 44 J/g. X-ray powder diffraction (XRPD) analysis of the resulting powder (see Supporting Information, Figure S2) confirms the presence of the PZQ–CU (2:1) cocrystal as the residual phase, validating the desolvation process. The melting point of the PZQ–CU (2:1) cocrystal was found to be T_{onset} = 129.51 °C, which is notably lower than the individual melting points of the parent compounds ($T_{melting}$ = 183 °C for curcumin; $T_{melting}$ = 136 °C for praziquantel). Degradation of the resulting melt occurs at approximately 190°C. Upon cooling, melting, and reheating, a glass transition occurs at $T_{midpoint}$ = 53.15°C. No (re)crystallization peaks were observed during temperature cycling.

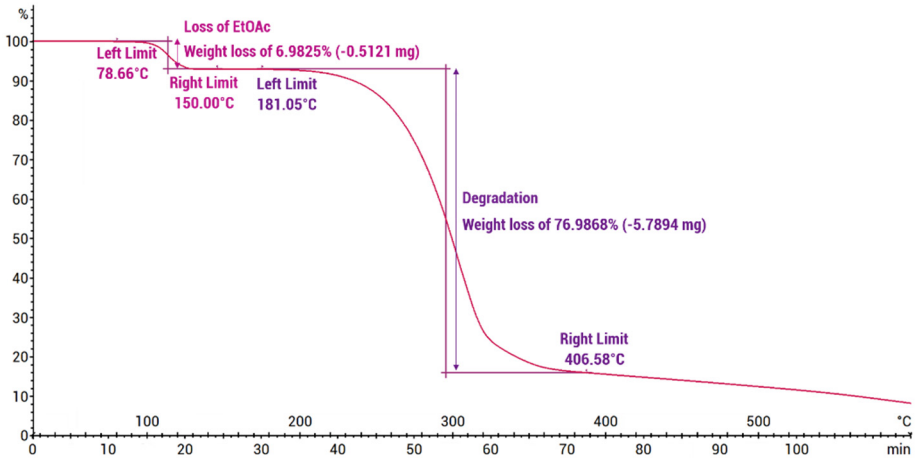


Figure 7. Thermogravimetric analysis of the PZQ–CU–EtOAc (2:1:1) cocrystal solvate obtained via slurry in ethyl acetate (initial sample mass: 7.5200 mg), expressed in weight (%) as a function of temperature (°C) and time (min).

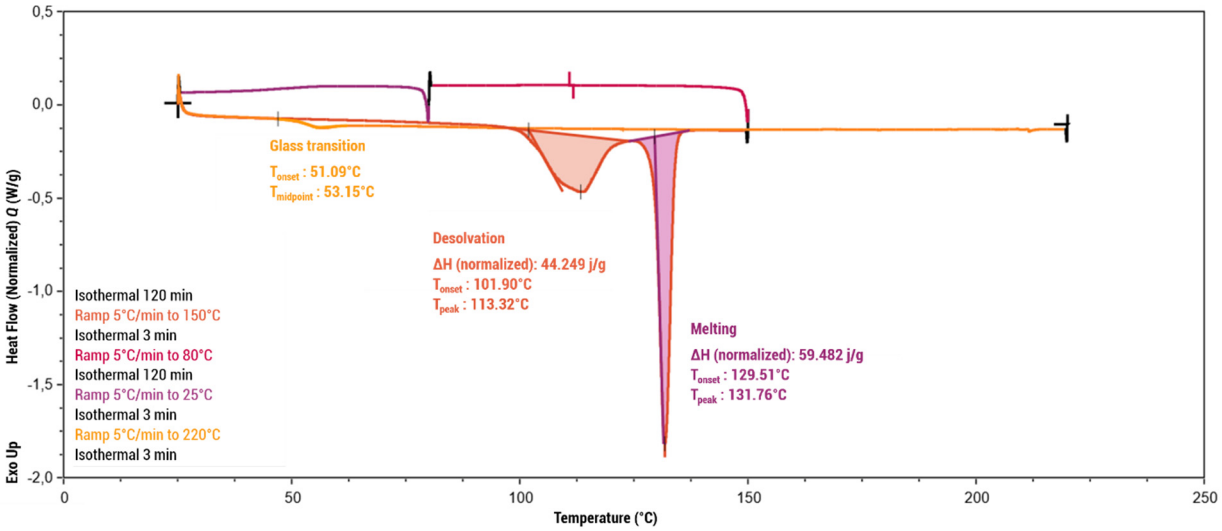


Figure 8. Differential scanning calorimetry analysis of the PZQ–CU–EtOAc (2:1:1) cocrystal solvate obtained via slurry in ethyl acetate, expressed in mW as a function of temperature (°C).

Furthermore, VT-XRD experiments were performed between RT and 121.85 °C (395 K), revealing the gradual change from the (2:1:1) cocrystal solvate to the desolvated (2:1) cocrystal, providing valuable insight into thermal behaviors and phase evolution. Figure 9 illustrates that the simulated diffraction pattern of the single crystal structure (SC_RT) determined at room temperature is similar to the PXRD pattern at 296 K (RT). At 380 K, the peak at 6.45° starts to disappear, while the peak at 6° shifts toward lower angles, indicative of changes in the unit cell parameters. Also, the characteristic peak of the desolvated

phase emerges at 6.7°, signifying the formation of the distinct phase. At 395 K, the phase transformation is complete, and the PXRD patterns closely resemble the 2:1 desolvated structure (SC_HT). This closely matches the observed temperatures in DSC and TGA. The difference in the reported desolvation temperatures can be attributed to the absence of carrier gas in the case of the VT-PXRD performed within a closed capillary.

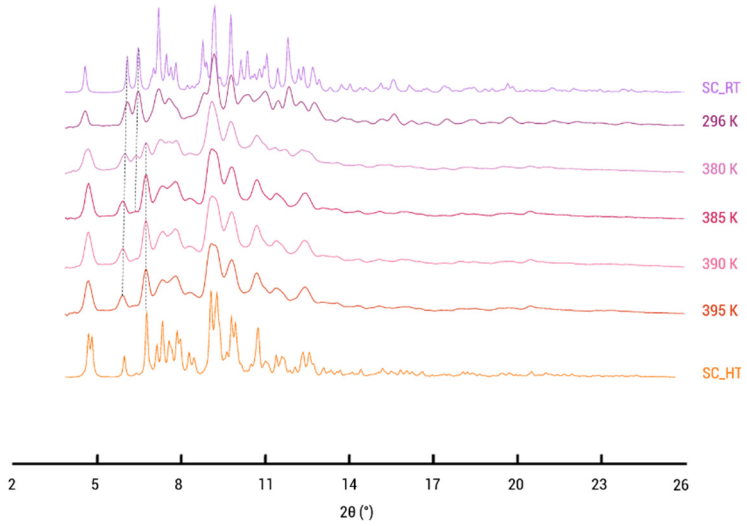


Figure 9. Variable-temperature X-ray powder diffraction patterns of PZQ–CU–EtOAc (2:1:1) cocrystal solvate. The temperature range is from 296 K to 395 K.

4. Conclusions

In this study, we investigated the co-crystallization potential between praziquantel (PZQ) and curcumin (CU), allowing us to identify two new solid forms: a cocrystal solvate and a non-solvated cocrystal. Here, we have successfully highlighted the potential of crystal engineering to combine a drug and a nutraceutical.

Further investigation and experiment, such as single crystal analysis, confirmed the formation of a praziquantel–curcumin–ethyl acetate (2:1:1) cocrystal solvate as well as a praziquantel–curcumin (2:1) cocrystal, obtained via solvent loss. Upon heating, the cocrystal solvate loses ethyl acetate molecules occupying voids with minimal interaction within the crystal lattice, and transition to a non-solvated cocrystal occurs. Comparing the solvate and non-solvated structures, only subtle differences in solid-state arrangements occur.

Thermal analyses revealed that the cocrystal solvate remains stable up to approximately 100 °C, at which point a transition to the non-solvated phase occurs. This latter one melts at 130 °C, which is a lower melting point compared to the individual components.

VT-XRPD experiments, conducted over the temperature range from RT to 395 K, elucidated the thermal behaviors and phase transition from the (2:1:1) cocrystal solvate to the desolvated (2:1) cocrystal. The close alignment of the results with temperatures observed in DSC and TGA emphasizes the importance of the experimental conditions, particularly the absence of carrier gas in VT-XRPD conducted within a closed capillary.

Exploring the impact of curcumin on the bitterness of praziquantel, as well as its potential mitigating effects on the adverse reactions associated with the drug in the cocrystal, would be of scientific interest for future applications.

In conclusion, here, we showcase a new praziquantel–nutraceutical cocrystal, which, furthermore, can be obtained as a stable solvate cocrystal, with potential implications for pharmaceutical applications.

Supplementary Materials: The following supporting information can be downloaded at: https://www.mdpi.com/article/10.3390/cryst14020181/s1.

Author Contributions: The manuscript was written with contributions from all authors. All authors have read and agreed to the published version of the manuscript.

Funding: This work was funded by Actions de Recherche Concerté (ARC) under the project PURE-20/25-108—New approaches in Process Intensification: Towards combined PUrefication-REaction Membrane based processes and the Fonds de la Recherche Scientifique (FNRS) CDR J.0168.22.

Data Availability Statement: CCDC 2309015-2309017 contain the supplementary crystallographic data for this paper. These data can be obtained free of charge from The Cambridge Crystallographic Data Centre via www.ccdc.cam.ac.uk/structures.

Acknowledgments: This work was funded by Actions de Recherche Concerté (ARC) under the project PURE- 20/25-108—New approaches in Process Intensification: Towards combined PUrefication-REaction Membrane based processes.

Conflicts of Interest: The authors declare no conflict of interest.

References

1. McManus, D.P.; Dunne, D.W.; Sacko, M.; Utzinger, J.; Vennervald, B.J.; Zhou, X.-N. Schistosomiasis. *Nat. Rev. Dis. Primers* **2018**, *4*, 13. [CrossRef] [PubMed]
2. Colley, D.G.; Bustinduy, A.L.; Secor, W.E.; King, C.H. Human Schistosomiasis. *Lancet* **2014**, *383*, 2253–2264. [CrossRef] [PubMed]
3. Kokaliaris, C.; Garba, A.; Matuska, M.; Bronzan, R.N.; Colley, D.G.; Dorkenoo, A.M.; Ekpo, U.F.; Fleming, F.M.; French, M.D.; Kabore, A.; et al. Effect of Preventive Chemotherapy with Praziquantel on Schistosomiasis among School-Aged Children in Sub-Saharan Africa: A Spatiotemporal Modelling Study. *Lancet Infect. Dis.* **2022**, *22*, 136–149. [CrossRef] [PubMed]
4. Schistosomiasis. Available online: https://www.who.int/news-room/fact-sheets/detail/schistosomiasis (accessed on 23 October 2023).
5. WHO Model Lists of Essential Medicines. Available online: https://www.who.int/groups/expert-committee-on-selection-and-use-of-essential-medicines/essential-medicines-lists (accessed on 5 July 2023).
6. Borrego-Sánchez, A.; Viseras, C.; Aguzzi, C.; Sainz-Díaz, C.I. Molecular and Crystal Structure of Praziquantel. Spectroscopic Properties and Crystal Polymorphism. *Eur. J. Pharm. Sci.* **2016**, *92*, 266–275. [CrossRef] [PubMed]
7. Meyer, T.; Sekljic, H.; Fuchs, S.; Bothe, H.; Schollmeyer, D.; Miculka, C. Taste, A New Incentive to Switch to (R)-Praziquantel in Schistosomiasis Treatment. *PLoS Neglected Trop. Dis.* **2009**, *3*, e357. [CrossRef] [PubMed]
8. Cappuccino, C.; Spoletti, E.; Renni, F.; Muntoni, E.; Keiser, J.; Voinovich, D.; Perissutti, B.; Lusi, M. Co-Crystalline Solid Solution Affords a High-Soluble and Fast-Absorbing Form of Praziquantel. *Mol. Pharm.* **2023**, *20*, 2009–2016. [CrossRef] [PubMed]
9. Navaratnam, A.M.D.; Sousa-Figueiredo, J.C.; Stothard, J.R.; Kabatereine, N.B.; Fenwick, A.; Mutumba-Nakalembe, M.J. Efficacy of Praziquantel Syrup versus Crushed Praziquantel Tablets in the Treatment of Intestinal Schistosomiasis in Ugandan Preschool Children, with Observation on Compliance and Safety. *Trans. R. Soc. Trop. Med. Hyg.* **2012**, *106*, 400–407. [CrossRef]
10. Babu, N.J.; Nangia, A. Solubility Advantage of Amorphous Drugs and Pharmaceutical Cocrystals. *Cryst. Growth Des.* **2011**, *11*, 2662–2679. [CrossRef]
11. Bernstein, J. Polymorphism of Pharmaceuticals. In *Polymorphism in Molecular Crystals*, 1st ed.; Oxford University Press: New York, NY, USA, 2002; pp. 240–255.
12. Serajuddin, A.T.M. Salt Formation to Improve Drug Solubility. *Adv. Drug Deliv. Rev.* **2007**, *59*, 603–616. [CrossRef]
13. Good, D.J.; Rodríguez-Hornedo, N. Solubility Advantage of Pharmaceutical Cocrystals. *Cryst. Growth Des.* **2009**, *9*, 2252–2264. [CrossRef]
14. Espinosa-Lara, J.C.; Guzman-Villanueva, D.; Arenas-García, J.I.; Herrera-Ruiz, D.; Rivera-Islas, J.; Román-Bravo, P.; Morales-Rojas, H.; Höpfl, H. Cocrystals of Active Pharmaceutical Ingredients—Praziquantel in Combination with Oxalic, Malonic, Succinic, Maleic, Fumaric, Glutaric, Adipic, And Pimelic Acids. *Cryst. Growth Des.* **2013**, *13*, 169–185. [CrossRef]
15. Zanolla, D.; Perissutti, B.; Passerini, N.; Chierotti, M.R.; Hasa, D.; Voinovich, D.; Gigli, L.; Demitri, N.; Geremia, S.; Keiser, J.; et al. A New Soluble and Bioactive Polymorph of Praziquantel. *Eur. J. Pharm. Biopharm.* **2018**, *127*, 19–28. [CrossRef] [PubMed]
16. Zanolla, D.; Perissutti, B.; Vioglio, P.C.; Chierotti, M.R.; Gigli, L.; Demitri, N.; Passerini, N.; Albertini, B.; Franceschinis, E.; Keiser, J.; et al. Exploring Mechanochemical Parameters Using a DoE Approach: Crystal Structure Solution from Synchrotron XRPD and Characterization of a New Praziquantel Polymorph. *Eur. J. Pharm. Sci.* **2019**, *140*, 105084. [CrossRef] [PubMed]
17. Zanolla, D.; Hasa, D.; Arhangelskis, M.; Schneider-Rauber, G.; Chierotti, M.R.; Keiser, J.; Voinovich, D.; Jones, W.; Perissutti, B. Mechanochemical Formation of Racemic Praziquantel Hemihydrate with Improved Biopharmaceutical Properties. *Pharmaceutics* **2020**, *12*, 289. [CrossRef] [PubMed]
18. Zanolla, D.; Gigli, L.; Hasa, D.; Chierotti, M.R.; Arhangelskis, M.; Demitri, N.; Jones, W.; Voinovich, D.; Perissutti, B. Mechanochemical Synthesis and Physicochemical Characterization of Previously Unreported Praziquantel Solvates with 2-Pyrrolidone and Acetic Acid. *Pharmaceutics* **2021**, *13*, 1606. [CrossRef] [PubMed]
19. Sánchez-Guadarrama, O.; Mendoza-Navarro, F.; Cedillo-Cruz, A.; Jung-Cook, H.; Arenas-García, J.I.; Delgado-Díaz, A.; Herrera-Ruiz, D.; Morales-Rojas, H.; Höpfl, H. Chiral Resolution of RS-Praziquantel via Diastereomeric Co-Crystal Pair Formation with l-Malic Acid. *Cryst. Growth Des.* **2016**, *16*, 307–314. [CrossRef]

20. Devogelaer, J.-J.; Charpentier, M.D.; Tijink, A.; Dupray, V.; Coquerel, G.; Johnston, K.; Meekes, H.; Tinnemans, P.; Vlieg, E.; Ter Horst, J.H.; et al. Cocrystals of Praziquantel: Discovery by Network-Based Link Prediction. *Cryst. Growth Des.* **2021**, *21*, 3428–3437. [CrossRef]
21. Yang, D.; Cao, J.; Heng, T.; Xing, C.; Yang, S.; Zhang, L.; Lu, Y.; Du, G. Theoretical Calculation and Structural Analysis of the Cocrystals of Three Flavonols with Praziquantel. *Cryst. Growth Des.* **2021**, *21*, 2292–2300. [CrossRef]
22. Liu, Q.; Yang, D.; Chen, T.; Zhang, B.; Xing, C.; Zhang, L.; Lu, Y.; Du, G. Insights into the Solubility and Structural Features of Four Praziquantel Cocrystals. *Cryst. Growth Des.* **2021**, *21*, 6321–6331. [CrossRef]
23. Rodríguez-Ruiz, C.; Salas-Zúñiga, R.; Sánchez-Guadarrama, M.O.; Delgado-Díaz, A.; Herrera-Ruiz, D.; Morales-Rojas, H.; Höpfl, H. Structural, Physicochemical, and Biopharmaceutical Properties of Cocrystals with RS- and R-Praziquantel—Generation and Prolongation of the Supersaturation State in the Presence of Cellulosic Polymers. *Cryst. Growth Des.* **2022**, *22*, 6023–6038. [CrossRef]
24. Yang, S.; Liu, Q.; Ji, W.; An, Q.; Song, J.; Xing, C.; Yang, D.; Zhang, L.; Lu, Y.; Du, G. Cocrystals of Praziquantel with Phenolic Acids: Discovery, Characterization, and Evaluation. *Molecules* **2022**, *27*, 2022. [CrossRef] [PubMed]
25. Esatbeyoglu, T.; Huebbe, P.; Ernst, I.M.A.; Chin, D.; Wagner, A.E.; Rimbach, G. Curcumin—From Molecule to Biological Function. *Angew. Chem. Int. Ed.* **2012**, *51*, 5308–5332. [CrossRef]
26. Kotha, R.R.; Luthria, D.L. Curcumin: Biological, Pharmaceutical, Nutraceutical, and Analytical Aspects. *Molecules* **2019**, *24*, 2930. [CrossRef] [PubMed]
27. Kharat, M.; Du, Z.; Zhang, G.; McClements, D.J. Physical and Chemical Stability of Curcumin in Aqueous Solutions and Emulsions: Impact of PH, Temperature, and Molecular Environment. *J. Agric. Food Chem.* **2017**, *65*, 1525–1532. [CrossRef] [PubMed]
28. Kunnumakkara, A.B.; Bordoloi, D.; Padmavathi, G.; Monisha, J.; Roy, N.K.; Prasad, S.; Aggarwal, B.B. Curcumin, the Golden Nutraceutical: Multitargeting for Multiple Chronic Diseases. *Br. J. Pharmacol.* **2017**, *174*, 1325–1348. [CrossRef] [PubMed]
29. Sharifi-Rad, J.; Rayess, Y.E.; Rizk, A.A.; Sadaka, C.; Zgheib, R.; Zam, W.; Sestito, S.; Rapposelli, S.; Neffe-Skocińska, K.; Zielińska, D.; et al. Turmeric and Its Major Compound Curcumin on Health: Bioactive Effects and Safety Profiles for Food, Pharmaceutical, Biotechnological and Medicinal Applications. *Front. Pharmacol.* **2020**, *11*, 01021. [CrossRef] [PubMed]
30. Canistro, D.; Chiavaroli, A.; Cicia, D.; Cimino, F.; Curro, D.; Dell'Agli, M.; Ferrante, C.; Giovannelli, L.; Leone, S.; Martinelli, G. The Pharmacological Basis of the Curcumin Nutraceutical Uses: An Update. *Pharmadvances* **2021**, *3*, 421–466. [CrossRef]
31. Tabanelli, R.; Brogi, S.; Calderone, V. Improving Curcumin Bioavailability: Current Strategies and Future Perspectives. *Pharmaceutics* **2021**, *13*, 1715. [CrossRef]
32. Sanphui, P.; Goud, N.R.; Khandavilli, U.R.; Nangia, A. Fast Dissolving Curcumin Cocrystals. *Cryst. Growth Des.* **2011**, *11*, 4135–4145. [CrossRef]
33. Rathi, N.; Paradkar, A.; Gaikar, V.G. Polymorphs of Curcumin and Its Cocrystals with Cinnamic Acid. *J. Pharm. Sci.* **2019**, *108*, 2505–2516. [CrossRef]
34. Dal Magro, C.; dos Santos, A.E.; Ribas, M.M.; Aguiar, G.P.S.; Volfe, C.R.B.; Lopes, M.L.L.C.; Siebel, A.M.; Müller, L.G.; Bortoluzzi, A.J.; Lanza, M.; et al. Production of Curcumin-Resveratrol Cocrystal Using Cocrystallization with Supercritical Solvent. *J. Supercrit. Fluids* **2021**, *171*, 105190. [CrossRef]
35. Sathisaran, I.; Dalvi, S.V. Crystal Engineering of Curcumin with Salicylic Acid and Hydroxyquinol as Coformers. *Cryst. Growth Des.* **2017**, *17*, 3974–3988. [CrossRef]
36. Thakuria, R.; Sarma, B. Drug-Drug and Drug-Nutraceutical Cocrystal/Salt as Alternative Medicine for Combination Therapy: A Crystal Engineering Approach. *Crystals* **2018**, *8*, 101. [CrossRef]
37. Sinha, A.S.; Maguire, A.R.; Lawrence, S.E. Cocrystallization of Nutraceuticals. *Cryst. Growth Des.* **2015**, *15*, 984–1009. [CrossRef]
38. Macrae, C.F.; Sovago, I.; Cottrell, S.J.; Galek, P.T.A.; McCabe, P.; Pidcock, E.; Platings, M.; Shields, G.P.; Stevens, J.S.; Towler, M.; et al. Mercury 4.0: From Visualization to Analysis, Design and Prediction. *J. Appl. Crystallogr.* **2020**, *56*, 226–235. [CrossRef] [PubMed]
39. Roisnel, T.; Rodríquez-Carvajal, J. WinPLOTR: A Windows Tool for Powder Diffraction Pattern Analysis. *Mater. Sci. Forum* **2001**, *378–381*, 118–123. [CrossRef]
40. Rigaku Oxford Diffraction. *CrysalisPro Software System, Version 1.171.38.41l*; Rigaku Oxford Diffraction Ltd.: Oxford, UK, 2015.
41. Sheldrick, G.M. XS, version 2013/1; Georg-August-Universität Göttingen: Göttingen, Germany. Sheldrick, G.M. SHELXT—Integrated Space-Group and Crystal-Structure Determination. *Acta Crystallogr. Sect. A Found. Adv.* **2015**, *71*, 3–8. [CrossRef] [PubMed]
42. Sheldrick, G.M. Crystal Structure Refinement with SHELXL. *Acta Crystallogr. Sect. C Struct. Chem.* **2015**, *71*, 3–8. [CrossRef]
43. Spek, A.L. Structure Validation in Chemical Crystallography. *Acta Crystallogr. Sect. D Biol. Crystallogr.* **2009**, *65*, 148–155. [CrossRef]
44. Etter, M.C. Encoding and Decoding Hydrogen-Bond Patterns of Organic Compounds. *Acc. Chem. Res.* **1990**, *23*, 120–126. [CrossRef]

Disclaimer/Publisher's Note: The statements, opinions and data contained in all publications are solely those of the individual author(s) and contributor(s) and not of MDPI and/or the editor(s). MDPI and/or the editor(s) disclaim responsibility for any injury to people or property resulting from any ideas, methods, instructions or products referred to in the content.